Lab on a Chip

PAPER

View Article Online
View Journal | View Issue

Cite this: *Lab Chip*, 2025, **25**, 6231

Gravity-perfused airway-on-a-chip optimized for quantitative BSL-3 studies of SARS-CoV-2 infection: barrier permeability, cytokine production, immunohistochemistry, and viral load assays

Shannon L. Faley,[ab] Niloufar A. Boghdeh,[c] David K. Schaffer,[ad] Eric C. Spivey,[ab] Farhang Alem,[c] Aarthi Narayanan,[ce] John P. Wikswo *[abdf] and Jacquelyn A. Brown[ad]

Received 23rd May 2025,
Accepted 16th September 2025

DOI: 10.1039/d5lc00510h

rsc.li/loc

Human microphysiological systems, such as organs on chips, are an emerging technology for modeling human physiology in a preclinical setting to understand the mechanism of action of drugs, to evaluate the efficacy of treatment options for human disease and impairment, and to assess drug toxicity. By using human cells co-cultured in three-dimensional constructs, organ chips can provide greater fidelity to the human cellular condition than their two-dimensional predecessors. However, with the rise of SARS-CoV-2 and the global COVID-19 pandemic, it became clear that many microphysiological systems were not compatible with or optimized for studies of infectious disease and operation in a Biosafety Level 3 (BSL-3) environment. Given that one of the early sites of SARS-CoV-2 infection is the airway, we created a human airway organ chip that could operate in a BSL-3 space with high throughput and minimal manipulation, while retaining the necessary physical and physiological components to recapitulate tissue response to infectious agents and the immune response to infection.

1. Introduction

With the highly contagious respiratory infection of SARS-CoV-2 sweeping the globe more than once and respiratory disease being one of the most common causes of morbidity and mortality worldwide,[1] we can well understand why interest in modeling the human respiratory tract has reached an all-time high. Essential features that must be recapitulated include human cells, an air–liquid interface, co-culture of multiple cell types mimicking native airway architecture, and immune cell activation and recruitment, as well as compatibility with Biosafety Level 3 (BSL-3) containment practices and ease of translation into labs that study infectious disease.[2] Clearly, the cells used for any infectious model are critical, as we were once again reminded in the case of SARS-CoV-2, where several promising drug candidates were advanced based on their efficacy in Vero cells. Unfortunately, these candidates showed no efficacy in human clinical trials, with the result that precious time and money were spent on compounds that had no future.[3–5] Animals may respond to a specific viral infection quite differently than humans, if at all,[6] and BSL-3 animal studies are particularly difficult and time consuming, and hence expensive. This in particular highlights the need for robust, early-stage *in vitro* cell models for candidate drug screening.

Microphysiological systems (MPS) have the potential to meet this need in several ways. The ability to use primary human cells from the relevant tissue type generates a model that better mimics the actual infection process in humans.[2] Another critical feature that MPS platforms can provide is the opportunity for an air–liquid interface that cannot be achieved with cellular monolayers on plastic.[7] Although a traditional cell culture of human airway epithelial cells can allow human cell–virus interaction, these cells fail to develop normally when cultured submerged in media.[8] Thus, to achieve a mature and more physiologically relevant airway epithelium requires the culture to have an air–liquid

[a] *Vanderbilt Institute for Integrative Biosystems Research and Education, Vanderbilt University, Nashville, TN 37235, USA*
[b] *Department of Biomedical Engineering, Vanderbilt University, Nashville, TN 37235, USA. E-mail: john.wikswo@vanderbilt.edu*
[c] *Biomedical Research Laboratory, Institute of Biohealth Innovation, George Mason University, Manassas, VA 20110, USA*
[d] *Department of Physics and Astronomy, Vanderbilt University, Nashville, TN 37235, USA*
[e] *College of Science, Department of Biology, George Mason University, Fairfax, VA 22030, USA*
[f] *Department of Molecular Physiology and Biophysics, Vanderbilt University, Nashville, TN 37232, USA*

interface, so that the air provides the necessary cues for development and there is still a feeding mechanism to maintain the cells. In addition, with an air–liquid interface, the epithelial cells are not in contact with cell media but instead exchange nutrients and metabolites across a porous membrane whose opposite side supports a layer of endothelial cells that are in direct contact with flowing cell culture media. The continuous perfusion of the vascular side of a cellular barrier may wash away secreted inhibitors that would be active in a non-perfused Transwell®.[9] Hence, the MPS airway model requires not only an air–liquid interface but also perfusion and multiple cell types to provide the appropriate nourishment of the airway epithelium.[10,11] With an increased focus on response to infectious agents, MPS platforms could also include immune cell components so that the tissue would be able to respond directly and locally to the infectious agent, particularly with regard to cytokine production. An appropriately designed and implemented MPS model would create the microenvironment into which a candidate therapeutic could be introduced not only to human cells but also to a living epithelial/endothelial barrier well in advance of human clinical trials. Lastly, the design must be easy to use in the laboratory. In the case of infectious disease studies, there is a particular need for model systems that are compatible with the restrictions placed on a BSL-3 environment, the most pressing of which are the need for the system to be totally enclosed, so that no aerosols are released in the lab environment, and a hardware design that can withstand the rigours of decontamination for component reuse or repair.[12–16] These restrictions can be readily met with a compact, self-contained chip that needs neither extensive hardware nor external connections to transport fluids or air. Moreover, it should be straightforward to translate the platform into labs with expertise in infectious disease, but not necessarily in the use of microphysiological systems, so as to enable rapid drug screening and identification of therapeutic candidates that can be moved to more complex systems or animal models after passing these initial hurdles.

Several established pulmonary MPS platforms are readily used in a BSL-2 environment.[17–22] Transwell® and other organ chips have been used to study cellular effects of SARS-CoV-2 in BSL-3 labs.[23,24] There are multiple reports where SARS-CoV-2 is applied in a BSL-3 environment to an alveolar chip,[25–27] and a blood–brain barrier (BBB)-alveolus model.[28] An early study used a tissue-engineered microfluidic BBB model wherein needles were removed from a hydrogel-filled microfluidic device to create channels that were then lined with endothelial cells.[29] Plate-based vascular chips and a rocker system were used to study SARS-CoV-2 therapy.[30] As an example of how to meet the BSL-3 secondary containment criteria, Thacker *et al.* cultured primary human alveolar epithelial cells and human lung microvascular endothelial cells in an Emulate lung chip that was maintained in a sealed Tupperware box and perfused by a syringe pump.[31] A sophisticated, self-contained, automated well-plate system with on-board pumps and reservoirs supported 96 simultaneous drug-dosing experiments where epithelial cells were exposed to both SARS-CoV-2 and various drugs.[32,33] In non-viral cancer-related studies, gravity and a 4 mm reservoir height difference drove the perfusion of endothelial cells on a chip that recapitulated the perivascular niche.[34]

We have previously described our development of a microfluidic chip used to model the neurovascular unit (NVU),[35–37] consisting of two cellular chambers separated by a semipermeable membrane, with flow in both chambers driven by external syringe pumps that could support the high flow rates required for shear-force polarization of the brain microvascular endothelial cells. At the outset of the COVID-19 pandemic, we concluded that our pump-perfused platform and other organ chips that use pressurized reservoirs, pumps, and gravity feed, were ill-suited for BSL-3 use, with its strict rules regarding secondary containment and rigorous decontamination. In contrast to pseudovirus studies in microfluidic devices to quantify the binding of antiviral therapeutics to the spike protein,[21] which can be performed in BSL-2 facilities, study of the active SARS-CoV-2 pathogen requires BSL-3. Furthermore, no existing standalone gravity-fed organ chips can support for a full day the flow rates and hence shear forces required to polarize microvascular endothelial cells. Recognizing the various difficulties with translating existing MPS technologies into a BSL-3 environment, our group was determined to create a low-cost, standalone airway MPS that can be used in BSL-3 laboratories, particularly without tubing and external reservoirs or pumps. We well appreciate other challenges and roadblocks in the development, dissemination, and deployment of organ-chip models.[38–40]

Our criteria for optimization for BSL-3 use include: 1) compact design, preferably without any tubing or vertical platforms that would prevent complete secondary containment, since open reservoirs to the incubator space are not permissible and separated chips, reservoirs, and pumps connected with tubing increase the risk of leaks and accidental spills; 2) no bulky powered equipment, such as a rocker plate or pump perfusion, as this would take up valuable cell culture space and would both necessitate running power cords into the incubator, which is particularly undesirable in a higher containment facility, and also complicate decontamination of equipment for repair or at the end of an experiment; and 3) ease of use, for rapid adoption – the COVID-19 pandemic taught us that for infectious disease experts to adopt a new model or platform rapidly, it cannot have a steep learning curve if it is going to be widely deployed. Since microfluidic platforms already existed that were well suited for imaging studies, and because we were interested in transcriptomics, Western blots, ELISA, RNAseq, and mass spectrometry for gene expression, cytokine detection, proteomics, and metabolomics, we focused our airway chip design on achieving greater biomass and conditioned media volumes than are possible with MPS models whose cells are contained in a small microfluidic

channel. Also critical to our design was creating a simple, easy-to-use platform that was highly compatible with the restrictions of a BSL-3 environment and would allow greater throughput than is seen with many MPS platforms.

We now report a novel microfluidic barrier chip capable of gravity-driven perfusion at a high rate of flow that is readily used in either BSL-2 or BSL-3 without the need for external pumps, reservoirs, or tubing. We designed our gravity-flow chip with large enough reservoirs that we could maintain the requisite flow rates for at least 24 hours between the addition of new media and removal of the old, or longer if smaller channels were used to restrict the flow rate. This in turn required the development of deep, large area reservoirs that could be replica cast with PDMS, a prerequisite for bonding to both the channels and chambers of our previous barrier chip. In Fig. 2 and the associated text, we describe in complete detail the novel design considerations and protocols to cast these reservoirs with smooth surfaces for bonding to PDMS microfluidics and without bubbles trapped in the PDMS in the bottom or sides of the reservoirs.

We describe the application of this system for modeling the response of an airway epithelium to a SARS-CoV-2 infection; elsewhere we present results obtained when the chips were used to create a gravity-perfused NVU that was used in BSL-3 facilities to study alphavirus infections.[41] A key feature of our design is that these chips can be seeded and matured at the BSL-2 level and, when the chips demonstrate the appropriate physiological performance, they can be moved from BSL-2 into BSL-3 without the challenges of maintaining continuous perfusion during transfer, or the risks of biohazard release or the introduction of bubbles while disconnecting the chips from one perfusion system in BSL-2 and reconnecting the chips to another in BSL-3. Our approach thereby limits the time and space within BSL-3 to that required for infection and observation of the response, and it avoids either open handling of the chips or the transfer into BSL-3 of expensive hardware that cannot be readily removed for service or disposal.

2. Methods

2.1. Airway chip design, fabrication, and preparation

2.1.1. Design. The apical surface of human bronchial epithelial cells faces the airway lumen, while the basolateral surfaces are attached to adjacent cells and the basement membrane, in our case simulated by the ECM-coated filter membrane that separates the two chambers. *In vivo*, epithelial cells exhibit a stable and tightly maintained polarization that supports absorption, secretion, and the formation of an impermeable barrier. In contrast, the polarization of endothelial cells is more dynamic and context-dependent, with the apical surface exposed to the fluid-filled lumen of the endothelial tube and the basal surface to surrounding smooth muscle cells or extracellular matrix.[42–45] Our gravity-perfused chip has been designed specifically to ensure that fluid flow within the vascular compartment induces endothelial polarization, which may not occur in static Petri dishes or Transwell® cultures. In our context, the apical surfaces of both endothelial and epithelial layers are exposed to either the flowing media in the vascular and airway compartments or, later in the experiment, flowing media in the vascular compartment and air in the airway compartment, respectively. By definition, the basal surfaces of both cell types touch the extracellular matrix, *i.e.*, in our case, the opposite sides of the ECM-coated filter membrane.

The requirement of a high flow rate to induce shear-force polarization of human lung microvascular cells, and our desire to have a self-contained, gravity-perfused chip with passive fluid reservoirs that could operate for 24 hours with an acceptable range of flow rates, necessitated supply and collection reservoirs with a large horizontal area, lest the 24-hour changes in volume translate to significant changes in height and hence perfusion pressure. As shown in Fig. 1, the horizontal dimensions of the reservoirs were limited by the 5 cm width of the 5 cm by 10 cm microscope slide to which the fluidics were bonded. The reservoirs and their boundaries did not extend over the barrier region of the chip, so as not to interfere with obtaining high-quality images of the cells populating the barrier.

Unlike the pump-perfused NVU,[36,37] the growth area of this airway chip and the gravity NVU[41] were designed to be square, so that both sides of the membrane could be exposed to shear flow. This symmetry enables the gravity-driven flow to be more equal on both sides of the membrane, due to the fact that the fluidic resistance of the two flow chambers is nominally identical. This further means that reservoirs of comparable volume and dimension can be used to generate equivalent flow rates during the initial cell-seeding phase of cell growth, before the epithelial side is transitioned to airlift culture. All of these features contribute to the relative simplicity of the gravity-driven perfusion of our airway chip. The geometry of the flow chamber was modeled and optimized in conjunction with reservoir geometry in order to have the fluidic resistance necessary to provide ~2 μl min^{-1} mean volumetric flow rate, which has proven effective at inducing shear-driven tight junction formation in endothelial cells in the NVU.[41]

2.1.2. Manufacturing. Fabrication of the passive-perfusion reservoirs began with a custom mold set consisting of a cavity mold and a flat lid, separated from each other with 1 mm-thick spacers (Fig. 2A). The cavities that form the reservoir walls were machined into 12 mm-thick poly(methyl methacrylate) (PMMA) stock (McMaster Carr, Atlanta, GA, P/N 4615 T54) with a tapered end mill (McMaster Carr, P/N 8936A69) to a depth of 10 mm, with the 5° taper selected to ensure easy unmolding of the thick polydimethylsiloxane (PDMS) chamber from a deep mold. Demolding ports (Fig. 2B) were machined into the bottom of the cavity mold to aid in the removal of cured reservoirs from the mold. A second piece of PMMA was laser-cut and bonded to the top of the cavity mold to form a rim around its edge to contain

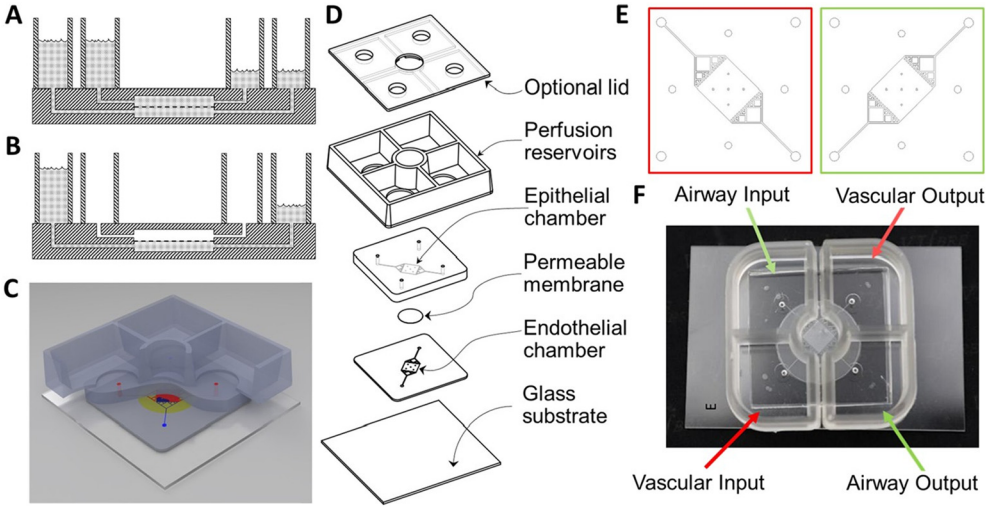

Fig. 1 Layout and design of airway chip for BSL-3 use. A) A schematic representation of a gravity-perfused airway chip with two chambers separated by a PET membrane (dashed line) and bonded inside the PDMS (hatched), with both chambers perfused by the difference in height of the media in the supply and collection chambers. B) An airway chip with the epithelial cells on the upper surface of the barrier membrane providing an air–liquid interface. C) An illustration of the complete chip. D) An exploded drawing of the airway chip. E) The mask layouts for the vascular (red) and airway (green) chambers and perfusion channels. F) A photograph of a completed airway chip with the reservoirs whose inlet–outlet height differences support gravity-driven perfusion in a BSL-3 space.

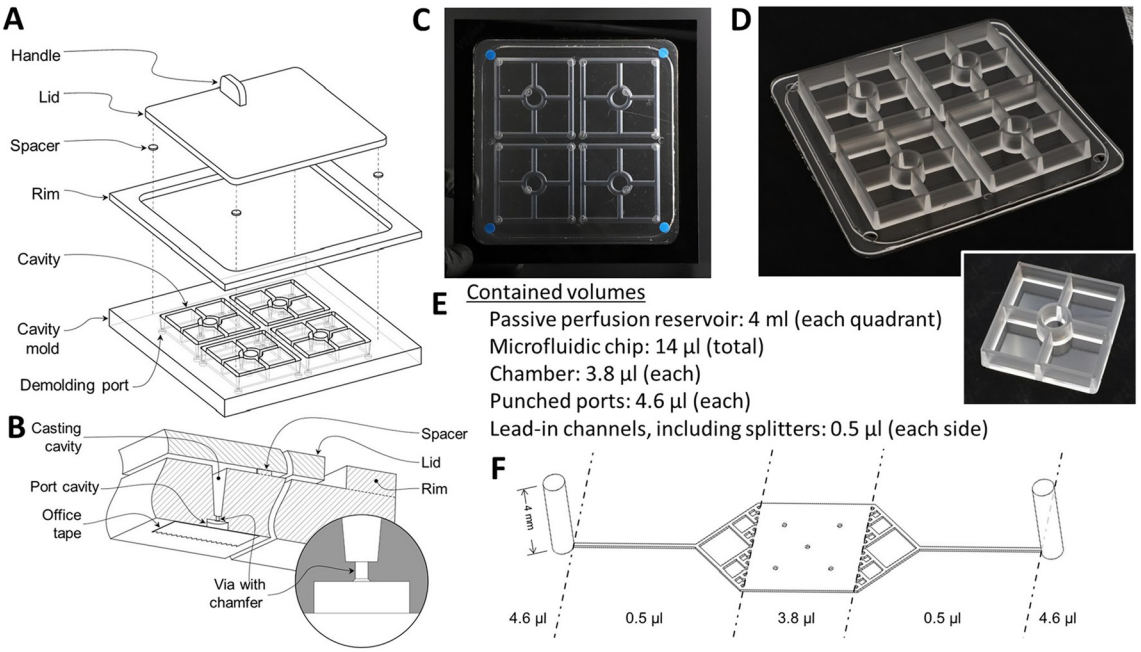

Fig. 2 Fabrication of the gravity-perfused airway chip. A) An exploded drawing of the mold used to cast the deep supply and collection reservoirs. B) Details of the cavities on the bottom of the mold that, upon removal of the small PDMS plug, allow pneumatic or hydraulic pressure to simplify extraction of the PDMS reservoir casting to be removed from the deep, tapered mold channels that form the sides of the reservoirs. C) A photograph of the PDMS-filled mold prior to parting. D) The cast PDMS piece after removal from the mold. Note that the four sets of reservoirs share a common, 1 mm thick bottom. The small, raised ring of PDMS near the edge is the overflow after an accurately measured volume of PDMS is poured into the open mold, degassed, and then displaced by the gradual lowering of the lid, with the excess PDMS being displaced into the gap between the lid and the rim. E) Airway chip volumes. F) Port, channel, splitter, and chamber volumes. The channels are 200 μm wide and 100 μm deep, and the chambers are 6.2 mm wide and 100 μm deep. The membrane between the two chambers has an area of 29 mm^2.

any overflow during the casting process. A third sheet of PMMA was laser-cut to serve as the lid for the cavity mold. A handle was affixed to the lid to assist in the casting process. Finally, PMMA spacers were cut, sanded to precise thickness, and bonded to the underside of the lid. Sylgard 184 PDMS (Dow Corning, Midland, MI) was mixed in a 10 : 1 ratio of base to curing agent using a Thinky Planetary Conditioning Mixer (Thinky, Tokyo, Japan, model AR-100). After covering

the demolding ports with self-adhesive office tape, the liquid PDMS was poured into the cavity mold and placed under vacuum for 10 minutes to remove any air bubbles. The lid was then lowered onto the surface strategically so as to prevent the capture of air between the mold parts (Fig. 2C). The PDMS was allowed to cure at room temperature for a minimum of 48 hours before demolding so that it would not cure into a thermally expanded mold, which would lead to the device being larger than desired upon cooling. Note the complete absence of bubbles in the cast chambers.

Forceps were used to remove the larger, cured PDMS plug filling the demolding port cavity (Fig. 2B), with the chamfer on the outer end of the via ensuring that the larger plug and the smaller one that connects it to the reservoir wall would separate as a unit that would be torn from the reservoir wall by the other, sharp via edge. Hence, the plugs can be separated from the molded reservoir wall without leaving a protruding fragment on the wall. Compressed air was injected through the demolding ports to part the reservoir casting from the mold. After demolding the reservoirs (Fig. 2D), flash was trimmed and a 12 mm diameter hole was punched from the floor of each quadrant using a biopsy punch (Difa Cooper, Milan, Italy).

The locations of the holes in the floors of the reservoirs match the access ports in the airway chip, which was cast using a similar molding approach, except that the channel and chamber pattern (Fig. 2F and S1) was created using a modified photolithography technique. Briefly, a 100 μm thick dry-film photoresist (SUEX 100, DJ Microlaminates, Sudbury, MA) was bonded to either a standard silicon wafer or a 22-gauge, #8 polished stainless steel wafer cut to fit a 120 mm square Petri dish (Stainless Supply, Monroe, NC). The pattern for the chip was exposed onto the dry film photoresist through a chrome-on-soda-lime glass photomask (Advanced Reproductions Corp., North Andover, MA). Once molded, the two halves of the airway chip were bonded together with a corona treatment system (Electro-Technic Products, Chicago, IL, model BD-20 AC).

To complete fabrication, the top surface of each airway chip and the bottom surface of each reservoir were also activated with corona treatment for 30 seconds, brought into contact with each other, and baked at 65 °C for a minimum of 4 hours. This process is very similar to the one used to create the gravity-flow neurovascular unit chips described previously.[41]

2.1.3. Preparation. Assembled airway chips were sterilized by gamma irradiation and stored in sealed bags at room temperature. To prepare for use, the airway chips were exposed to vacuum for 20 minutes up to 24 hours, then sterile water (Sigma, W3500500ML), prewarmed to 45 °C, was loaded *via* syringe into the vascular and airway chambers, taking care to avoid bubbles in the fluidic channels. The syringe assembly included a 1 ml Luer-Lok™ syringe (BD, Cat#: 309628) fitted with a blunt-tipped 23G needle (SAI, Cat#: B23-50) inserted into sterile (Tygon, 0.20 ID) tubing (Fisher Scientific, 14-171-284). The tubing was then pressure-fitted into the PDMS inlet channel. Chips were housed within T-150 resealable flasks (TPP, Cat# 91051), and 5 ml sterile water was added to the vascular and airway inlet reservoir chambers before placing the flasks on a level plate within the 37 °C incubator. To rinse any residual chemical byproducts from manufacturing that may leach from the PDMS molds, water was exchanged daily for 7 days by removing effluent *via* pipet from the exit chambers and adding fresh 45 °C sterile water to the inlet chambers. Chips were then coated with ECM solution *via* syringe, injecting at least 100 μl solution into both vascular and airway chambers, and allowed to incubate overnight at 37 °C. Once coated, the chips were rinsed with 1× PBS *via* syringe before loading EBM-2 media into the vascular chamber and B-ALI™ media into the airway chamber to further condition the PDMS for 24–48 hours prior to loading cells.

2.2. Cell and SARS-CoV-2 culture

All cells were maintained in BSL-2 facilities and incubated at 37 °C with 95% humidity and 5% CO_2.

2.2.1. Airway epithelial cells. Human bronchial/tracheal epithelial cells (normal human bronchial epithelial cells (NHBE), Lonza, Cat#: CC-2540S) were cultured in BSL-2 according to manufacturer's recommendations using B-ALI™ Bronchial Air-Liquid Interface Medium BulletKit™ (Lonza, Cat#: 00193514). Cells were initially seeded at a density of 3500 cells cm^2 in cell culture-treated T-75 flasks (ThermoFisher Scientific, Cat#: 10364131) with B-ALI™ Basal Media† (Lonza, Cat#: 00193514), and media was exchanged every 48 hours. Cells were passaged upon reaching 60% confluency using ReagentPack™ subculture reagents (Lonza, Cat#: CC-5034). Initial stocks were frozen in B-ALI™ Basal Media with 10% DMSO (Sigma, Cat# D2650) at P3 and P4 to ensure experimental consistency. To differentiate, NHBE cells were plated on 1 μm Transwell® inserts (Corning, Cat#: 353104) or loaded into airway chips (500 000 cells ml^1 and 1 × 10^6 cells ml^1, respectively) to achieve >80% confluence, and maintained in B-ALI™ Basal Media in both airway and vascular chambers. Once the monolayer reached >95% confluence (within 24–48 hours of seeding), Basal Media was removed from both chambers, and replaced with B-ALI Differentiation Media supplemented with 2 μl ml^{-1} freshly thawed B-ALI™ inducer in the vascular chamber only, to achieve airlift culture conditions. Basal Media was exchanged every 48 hours with B-ALI™ Differentiation Media supplemented with inducer for the remainder of the experiment. The airway chamber was rinsed with sterile 1× PBS (Gibco, Cat#: 10010023) every 3–4 days to thin mucous and remove cellular debris.

2.2.2. Vascular endothelial cells. Human lung microvascular endothelial cells (HMVEC-L, Lonza, Cat#: CC-2527) were cultured in BSL-2 according to manufacturer's recommendations using EGM™-2 MV Microvascular Endothelial Cell Growth Medium-2 BulletKit™ (Lonza, Cat#:

† Herein "Basal Media (or Medium)" recognizes the manufacturers' product names so as not to be confused with a particular side of the membrane.

CC-3202). Cells were initially seeded at a density of 10 000 cells cm^2 in cell culture-treated T-25 flasks (ThermoFisher Scientific, Cat#: 156367) with EGM™-2 media (Lonza, Cat#: 00193514), and media was exchanged every 48 hours. Cells were passaged upon reaching 90% confluency using ReagentPack™ subculture reagents (Lonza, Cat#: CC-5034). Initial stocks were frozen in EGM™-2 MV Basal Media with 10% DMSO (Sigma, Cat#: D2650) at P3 to ensure experimental consistency.

2.2.3. Generation of SARS-CoV-2 for infection. The SARS-Related Coronavirus 2 isolate Italy-INMI1 (NR-52284) was obtained from BEI Resources. The virus was propagated in BSL-3 according to the manufacturer's recommendation. Briefly, Vero cells were grown to about 70–80% confluency in a cell culture flask and infected with the stock virus (obtained from BEI Resources) at a multiplicity of infection (MOI) of 0.1. Once about 30–40% of the cells were exhibiting cytopathic effect (CPE), which was observed as cell rounding and sloughing, the supernatant was collected and titered by traditional plaque assay in Vero E6 cells (ATCC, Cat#: CRL-1586). The final viral titer was determined to be 1×10^6 PFU ml^{-1}.

2.3. Device loading and infection

2.3.1. Transwell® co-culture assembly. In BSL-2, a 100 μl ECM solution comprised of human placental collagen IV (Sigma, Cat#: C5533), fibronectin (Sigma, Cat#: F1141), and 1× PBS combined in a 4 : 1 : 5 ratio by volume, respectively, was applied to the airway and vascular chambers of 1 μm Transwell® inserts in 24-well plates (Corning, Cat#: 3527) and incubated at 37 °C overnight to coat. Transwell® membranes were then washed three times with 1× PBS prior to inversion of the inserts within the well plates. HMVEC-L cells were seeded on the vascular side of the inserts at a concentration of 100 000 cells ml^1 in EBM-2 media and allowed to incubate at 37 °C overnight to facilitate attachment. The inserts were then returned to an upright position with 500 μl EBM-2 media in the vascular chamber. NHBE cells were seeded at a density of 500 000 cells ml^1 of B-ALI™ Basal Media in the airway chamber and returned to a 37 °C incubator overnight. Once NHBE cells achieved >95% confluence in the airway chamber, all media was removed and replaced with 500 μl B-ALI™ Differentiation Media supplemented with 2 μl ml^{-1} inducer (Lonza, Cat#: 00193514) in the vascular chamber.

2.3.2. Airway chip cell loading. 100 μl HMVEC-L cells (Lonza, CC-2527) were loaded into the vascular chamber at a concentration of 500 000 cells ml^1 EBM-2 media *via* syringe assembly. The airway chips were inverted within a T-150 resealable flask housing and incubated overnight at 37 °C to allow attachment of the HMVEC cells to the vascular side of the membrane. They were then returned to an upright position and 5 ml EBM-2 media was added to the vascular inlet reservoir to initiate vascular flow. 100 μl of NHBE cells (Lonza, #CC-25410S) at a concentration of 1×10^6 cells ml^1 B-ALI™ Basal Media (Lonza, 00193516) were subsequently loaded *via* syringe assembly into the airway chamber and incubated overnight at 37 °C to facilitate attachment. 5 ml B-ALI™ Basal Media was then added to the airway chamber inlet reservoir to initiate flow. If the NHBE monolayer failed to achieve 95% confluency within 48 hours of initial seeding, the NHBE loading step was repeated.

2.3.3. Airway chip differentiation and maintenance. When the NHBE monolayer reached 95% confluency within the airway chamber, the airway chips were transitioned to airlift culture conditions. All media was removed from the inlet and exit reservoirs, as well as the airway chamber, *via* gentle suction with a 1000 μl pipet tip. 5 ml of B-ALI™ Differentiation Media (Lonza, 00193517) supplemented with B-ALI™ 2 μl ml^{-1} inducer (Lonza, Cat # (00193515) was added to the vascular chamber inlet reservoir only. For the first week, differentiation media was exchanged daily by removing effluent from the vascular exit reservoir and adding fresh media to the vascular inlet reservoir. Thereafter, media was exchanged every 48 hours for the duration of the experiment. Every 3–4 days, 1× PBS was added to the airway chamber inlet to rinse the NHBE cells of mucous and cellular debris.

2.3.4. Airway chip gravity perfusion. With gravity perfusion of organ chips, the differences in the height of the inlet and outlet reservoirs drive the flow of fluid through the cell-containing chambers of the chip, with the instantaneous flow rate being determined by both the height difference and the hydraulic resistance provided by the connecting channels and chambers. When this airway chip was being designed, the channel widths and lengths (Fig. 2F) and supply reservoir heights and volumes (Fig. 2E) were adjusted to provide a flow rate that would ensure steady flow for approximately 24 hours, thereby ensuring continued endothelial cell polarization as long as the outlet reservoirs were manually emptied and the inlet reservoir manually filled every day. Hence, gravity-driven perfusion is achieved by differences in the instantaneous height of a chamber's inlet and outlet reservoirs, as detailed in Fig. 1A and B. The flow rate of two microliters per minute is an average over 24 hours, as there is a decrease in flow rate over time. This average flow rate was both calculated based on the known dimensions and media volume heights and verified experimentally by weighing the effluent delivered to the initially empty outlet reservoir over the 24-hour time interval. Thus, we determined that the chip needed to be refreshed in terms of its flow every 24 hours by removal of output media and replenishment of input media for both the vascular chamber and, when appropriate, airway chambers. When both chambers are actively perfused as the endothelial and epithelial barriers are forming, there are minimal pressure gradients across the membrane.

2.3.5. Viral infection and sampling of airway chips. The process for infection and sampling is presented schematically in Fig. 3. The SARS-CoV-2 infection was carried out in BSL-3.

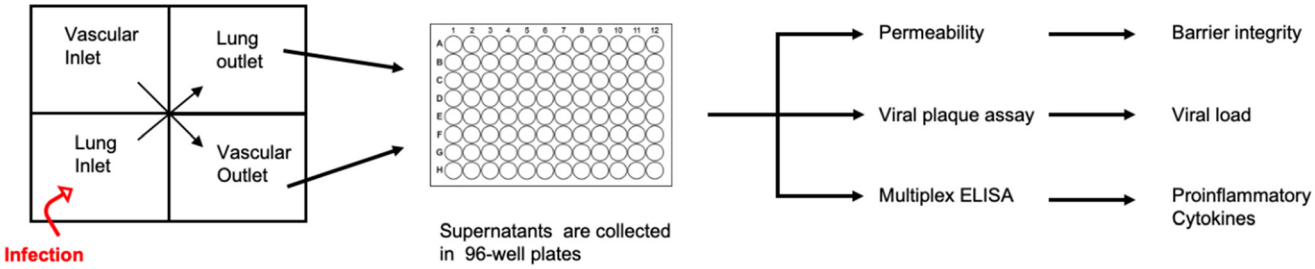

Fig. 3 A schematic representation of the steps for infection and sampling of the airway chip.

The virus was added to the perfusion medium to reach an MOI of 0.1 and introduced through the airway-side port of the airway chip. The virus-containing medium was continuously perfused into the airway chips overnight at 37 °C, 5% CO_2 conditions. For control chips, the usual medium was used for each chamber.

Twenty-four hours after the introduction of the virus into the chip, 100 μl of supernatant was collected from the vascular outlet chamber of each chip and collected in a 96-well white wall plate (100 μl per well, 3–4 times, total of 300–400 μl). Next, 100 μl of supernatant was collected from the basal outlet chamber of each chip and collected in a 96-well white wall plate (100 μl per well, 3–4 times, total of 300–400 μl). To resume gravity-driven perfusion, 1 mL of the appropriate medium was added to each of the inlet chambers.

This process was repeated over the course of the study, and all airway chips were maintained at 37 °C, 5% CO_2 in BSL-3 until the termination of the study. Supernatants were collected at 24, 48, 72, 120, and 168 hours post-infection from both chambers of all (control and infected) airway chips.

We note that at the time this work was performed, the Centers for Disease Control (CDC) required that SARS-CoV-2 studies be conducted in a BSL-3 laboratory. In December 2024, the CDC reduced the laboratory biosafety level for SARS-CoV-2 studies from BSL-3 to BSL-2.‡

2.4. Assays

We used a FITC-Dextran permeability measurement to determine the barrier integrity, a viral plaque assay to quantify the viral load, multiplex ELISA to report ACE-2, IL-6, and TNF-α, and Multiplex Micro ELISA to determine the proinflammatory cytokine profiles for vascular and basal cells.

2.4.1. Airway chip permeability assay. 10 kD FITC-Dextran (FD10S, Sigma-Aldrich) and 70 kD FITC-Dextran (FD70S, Sigma-Aldrich) were used to evaluate passive permeability in BSL-2 prior to transfer to BSL-3, and in BSL-3 post-infection. Stock solutions were made in water at 1 mM and stored at −80 °C. Working concentrations were prepared at 1 μM in Basal Medium. The vascular chambers were perfused *via* gravity, achieving an average flow rate of 2 μL min^{-1} over a 24-hour period. For passive permeability measurements, supernatant was collected from both vascular and airway chambers every day 24 hours after the last renewal of inlet media, and the difference in fluorescence intensity was analyzed using a plate reader (GloMax Microplate Reader, Promega). By measuring concentration in the airway and vascular chambers, the applied permeability coefficient was calculated using the standard equation[37,46,47] to calculate apparent permeability, $P_{aap} = (dQ/dt) \times 1/AC$, where dQ/dt is the change in concentration per unit time at steady state, A is the growth area (33 mm^2 in the Transwell® and 29 mm^2 in the airway chip), and C is the initial concentration in the airway chamber.

2.4.2. Plaque assay for viral infection. In BSL-3, quantification of infectious virus titer by plaque assay was performed in Vero E6-TMPRSS2 cells (kindly provided by Dr. Shirit Einav, Stanford University). TMPRSS2 cells were seeded in 12-well plates at 1.5×10^5 cells per well.

A ten-fold serial dilution (from 10^1 to 10^6) was performed using 30 μL of supernatant collected from all timepoints at both the vascular and airway outlets. Each 30 μL sample was diluted into 270 μL of Eagle's Minimum Essential Medium (EMEM; ATCC, Cat. 30-2003) supplemented with 10% Fetal Bovine Serum (Corning, Cat. 35-010-CV) and 2% Geneticin (Life Technologies, Cat. 10131027). Then, 200 μL of each dilution was used to infect TMPRSS2 cells in 12-well plates for 1 hour.

At one hour post-infection, 1 ml per well overlay of a 1 : 1 solution of 0.6% agarose in distilled H_2O with 2× Eagle's minimal essential medium (Quality Biological, Cat#: 115-073-101) was added to cells and allowed to solidify at room temperature. The plates were subsequently transferred to 37 °C, 5% CO_2 culture conditions and maintained for up to 72 hours post-infection.

After 72 hours, the TMPRSS2 plates were fixed with 1 ml per well of 10% formaldehyde at room temperature. Approximately 24 hours after fixation, formaldehyde and the agar plugs were removed, and fixed cells were stained with 1% crystal violet in 20% methanol solution for 15 minutes.

‡ In December 2024, the CDC revised the Laboratory Biosafety Guidelines for working with SARS-CoV-2 (**https://www.cdc.gov/covid/php/lab/index.html**), with the qualifier that "[t]his revised guidance is specific to SARS-CoV-2 and should not be extrapolated to other members of the *Coronaviridae* family or to other members of the species *Betacoronavirus pandemicum*." In part, the guidelines state that "[a]t a minimum, BSL-2 facilities, practices, and procedures are recommended for diagnostic research, anatomic pathology, environmental, and virus propagation activities utilizing SARS-CoV-2."

We counted plaques for each plate and calculated plaque-forming units per mL (PFU mL^{-1}) for each sample. The mean and standard deviation were determined using an average of three replicates for each sample.

2.4.3. Transwell® fixation and staining. Transwell® plates were rinsed three times with 500 μl 1× PBS for five minutes at room temperature. Cells were fixed by application of 100 μl undiluted Cytofix solution (BD Biosciences, Cat#: 554714) and incubated at room temperature for 15 minutes before rinsing three times with Cytoperm solution (BD Biosciences, Cat#: 554714) diluted 1 : 10 in 1× PBS for five minutes. Cells were blocked with 500 μl 1× PBS containing 2% goat serum (Thermo-Fisher Scientific, Cat#: PCN5000) and incubated overnight at 4 °C.

2.4.4. Airway chip fixation and staining. All media was removed from the inlet and outlet chambers prior to gently flushing 200 μl 1× PBS *via* syringe assembly through each cellular chamber. The inlet chambers were then filled with 5 ml 1× PBS and allowed to flow *via* gravity for a minimum of 15 minutes at room temperature. All fluid was removed before introducing 100 μl Cytofix (Fisher Scientific, BDB554722) solution *via* syringe assembly and incubating at room temperature for 15 minutes. Chambers were then washed by first gently introducing 200 μl Cytoperm diluted 1 : 10 in 1× PBS *via* syringe assembly. Inlet chambers were filled with 5 ml Cytoperm solution and allowed to flow *via* gravity at room temperature for at least 15 minutes. Cells were blocked by removing the Cytoperm solution, then filling the inlet chambers with 5 ml 1× PBS with 2% goat serum and incubating overnight at 4 °C. Cells were then labeled with antibodies diluted in 1× PBS with 2% goat serum and allowed to incubate overnight at 4 °C (Table S1), followed by a final wash with 1× PBS before imaging.

2.4.5. Micro-ELISA. The perfused media from the airway and the vascular sides of the units (infected [$N = 3$], control, [$N = 3$]) were collected at 24, 48, 72, 120, and 168 hours post-infection. We performed ELISA cytokine analysis on 50 μl effluent samples using the V-Plex Human Cytokine Kit (Meso Scale Discovery, Rockville, MD, USA), which measured ten cytokines (IFN-γ, IL-1β, IL-2, IL-4, IL-6, IL-8, IL-10, IL12-p70, IL13, and TNF-α). Sample preparation was carried out as described previously.[46]

2.4.6. ELISA. ELISA for ACE-2 (AbCam Waltham, MA), IL-6, and TNF-α (ThermoFisher Waltham, MA) samples were prepared and run according to the manufacturer's recommendation for each ELISA cytokine kit.

2.5. Statistical analysis and data processing

All quantifications were performed by incorporating data obtained from triplicate samples unless indicated otherwise. Error bars in all figures indicate standard deviations. Plaque assay and proinflammatory cytokine data calculations were performed using Microsoft Excel. Graphs and *P*-values were designed and calculated using GraphPad Prism version 10.0.0 for MacOS. Significance values are from two-way ANOVA with Dunnett's post-test or unpaired two-tailed *t*-test and are indicated using asterisks: $*p < 0.05$, $**p < 0.01$, $***p < 0.001$, $****p < 0.0001$.

3. Results

The following results have allowed us to assess both the maturation of our airway chips in a BSL-2 environment and their ability to recapitulate in a BSL-3 environment, the infection of the human airway with the SARS-CoV-2 virus, thereby demonstrating that gravity-perfused airway chips can be used to study viral infections over the course of several days with minimal complications in translating our MPS technology from BSL-2 to BSL-3 environments.

3.1. NHBE maturation under static, Transwell® conditions

We performed initial validation experiments to verify the ability to generate an airway model comprising vascular and airway epithelial components under static conditions by culturing NHBE and HMVEC-L cells on the airway and vascular surfaces, respectively, and assessing cellular markers and functional indicators of maturation over time.

Maturation of a pseudostratified, polarized epithelium, typified by mucin-producing goblet cells and ciliated columnar cells, was analyzed through antibody staining of cellular markers cadherin-26 (CDH26, Fig. 4A), VANGL1 (Fig. 4B), MU5AC (mucin, Fig. 4C), and alpha-tubulin (Fig. 4D) on days 0, 14, and 28 after airlift. In each case, staining profiles intensified over time with maximal expression observed after four weeks of culture. Next, we assessed the permeability of the co-cultures to 330 Da sodium fluorescein over time. Fig. 4E shows that co-culture conditions resulted in markedly decreased permeability as compared to HMVEC-L (1.36×10^{-5} cm s^{-1}) and NHBE (2.35×10^{-5} cm s^{-1}) monolayers, emphasizing the importance of the synergism between vascular and epithelial layers in the development of the airway model. Fig. 4F shows that the barrier strengthened from 1.85×10^{-5} cm s^{-1} on day 0 to 7.83×10^{-6} cm s^{-1} on day 28 after airlift, providing evidence of increasing robustness of intercellular junctional integrity with maturation. Finally, we compared monolayer permeability to sodium fluorescein to co-culture assemblies after 28 days (NHBE and co-culture samples were maintained under airlift conditions).

3.2. Co-culture in airway chips

We sought to demonstrate the ability to reproduce the static Transwell® airway model within a microphysiological platform subjected to continuous gravity-driven perfusion. Fig. 5A shows the permeability of airway chips to sodium fluorescein on days 0 and 30 after airlift, decreasing from 4.9×10^{-6} cm s^{-1} to 1.4×10^{-6} cm s^{-1}, as compared to 7.83×10^{-6} cm s^{-1} to 1.98×10^{-6} cm s^{-1} in Transwell®. For the Transwell® data in Fig. 4A, the ratio of day 0 permeability to day 28 permeability was 2.5. For the gravity-perfused chip,

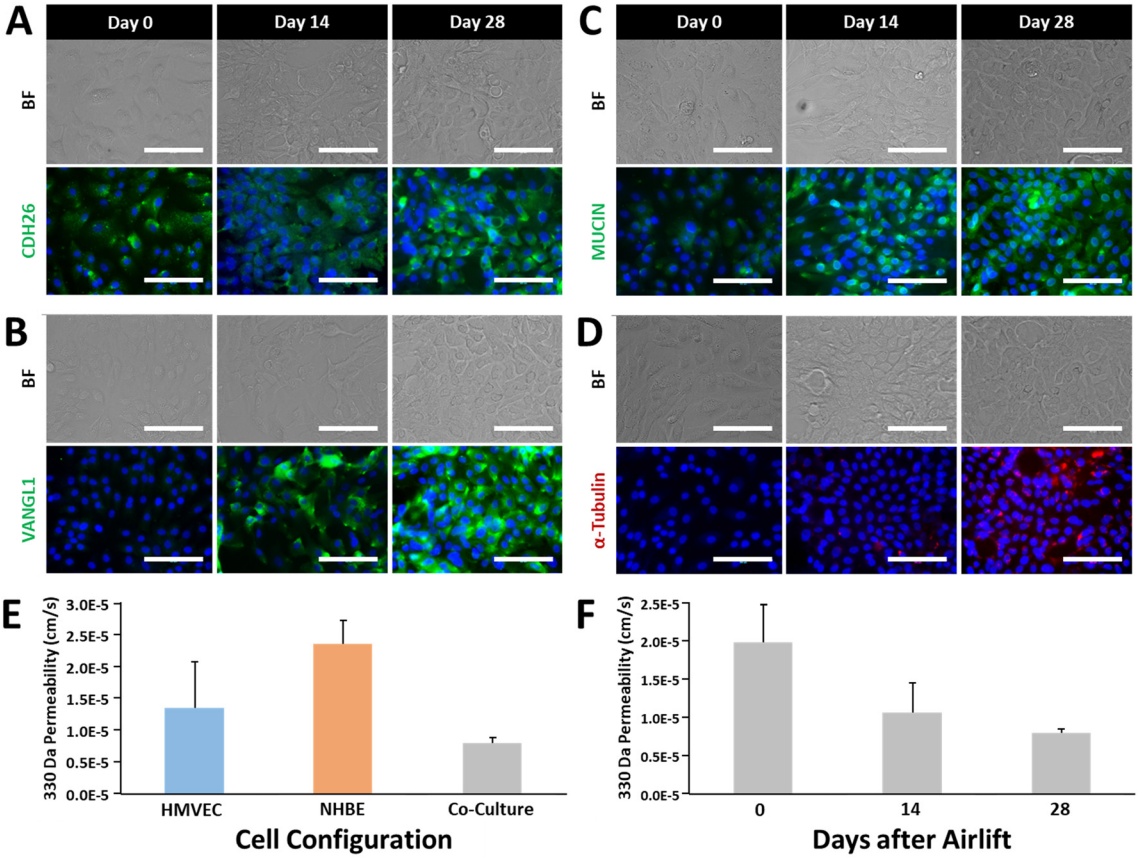

Fig. 4 Maturation markers of airway epithelial development in a Transwell®. A) Cadherin-26 expression, which is associated with cell–cell junctions, epithelial integrity, and maturation, shows an increase in expression over time. B) VANGL1 is a planar cell polarity marker associated with barrier maturity that increases in expression over time as the airway epithelium develops. C). Mucin contributes to endothelial barrier function and its presence is a measure of barrier health. D) α-Tubulin is associated with cilia development and would indicate a well-differentiated epithelium within the bronchial area. E) Barrier permeability of airway cells in a Transwell® in mono- and co-culture after 28 days in culture. F) Airway barrier formation over time in a Transwell® containing both endothelial and epithelial airway cells.

the ratio of day 0 permeability to day 30 permeability in Fig. 5A was 3.5. The reciprocal of these numbers indicates that the day 28 Transwell® permeability was 40% of the day 0 value, and the day 30 permeability of the gravity-perfused airway chip was 28% of the day 0 value. We conclude that the perfused chips have tighter barriers than those of Transwell® cultures, and that our observed barrier strength increased during four weeks of maturation. Notably, the permeability values are lower with the 3D fluidic environment compared to static cultures at all time points. Note that because we have epithelial cells on one side of the membrane and endothelial cells on the other, we are unable to determine the relative contributions of the two cell types to this decrease in permeability. In our gravity-perfused neurovascular unit, permeability decreases were the result of flow-induced polarization of only endothelial cells.[41]

We also evaluated ACE-2 levels over time, as it has been well established that SARS-CoV-2 leverages ACE-2R to gain entry into cells.[48,49] Fig. 5B shows the concentration of soluble ACE-2 in the vascular and airway chamber effluent samples on days 15, 30, 45, and 60 after airlift, revealing a modest increase in ACE-2 secretion beginning after 45 days of culture. Although the platform configuration presents challenges in terms of imaging, we attempted to perform immunofluorescence assays of cellular markers associated with vascular integrity and pseudostratification of epithelial layers. In Fig. 5C, images show that the vascular (HMVEC-L) cells, which represent the endothelial layer of the airway chip, exhibit robust ZO-1 expression after 30 days post-airlift, demonstrating intact tight junctions. Likewise, epithelial layers (NHBE cells) positively stain MUCA5 (Mucin) and VANGL1 30 days after airlift (Fig. 5D).

3.3. Assessing the effects of cytokine stimulation on soluble ACE-2 concentrations

Given the critical importance of ACE-2 to SARS-CoV-2 infection and the relatively low concentration of soluble ACE-2 detected in previous experiments, we sought to determine whether cytokine stimulation of airway epithelial cell monolayers would increase soluble ACE-2 (sACE-2) levels. Two cytokine candidates, IL-33 (ref. 50) and IFN-gamma,[51] were identified from the literature as associated with, or likely to directly influence, elevated ACE-2 levels. Airway epithelial cells were cultured for 45 days on a Transwell® insert under airlift conditions, then exposed to

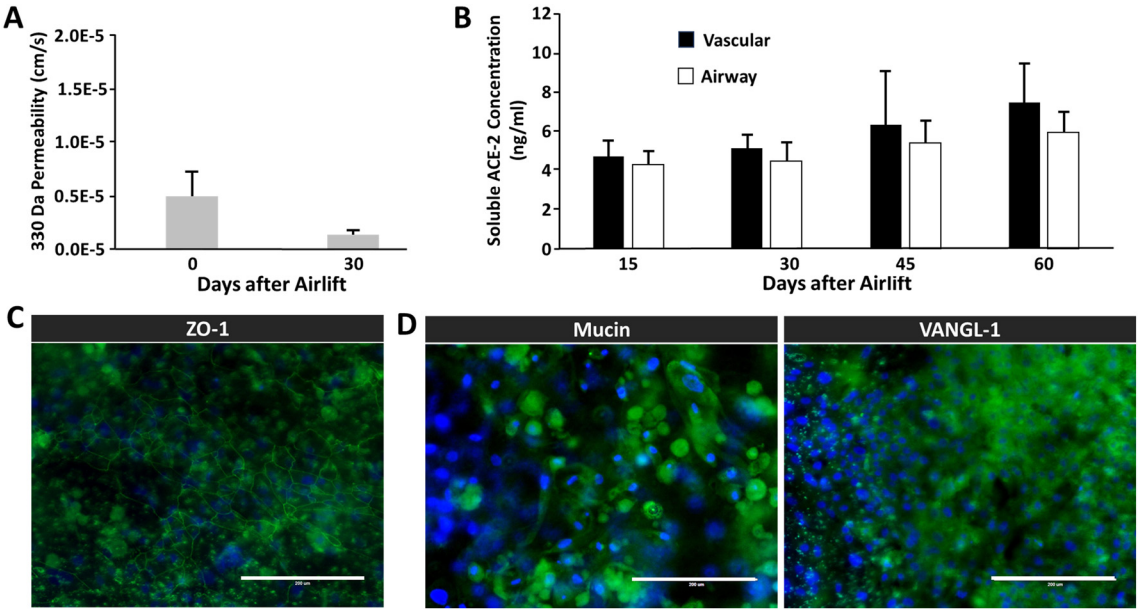

Fig. 5 Maturation of the co-culture airway chip. A) After 30 days, there is a functioning airway epithelial-to-vascular barrier, as shown by a significant decrease in permeability to small fluorescein (N = 9, p = 0.001). B) Detection of soluble ACE-2 is present after 15 days in culture in both vascular and epithelial effluent (N = 9). C) Maturation of the airway vascular endothelium shows junctional protein expression of Z0-1. D) Airway epithelium on the chip was also shown to have maturation markers previously described, including VANGL1 and mucin.

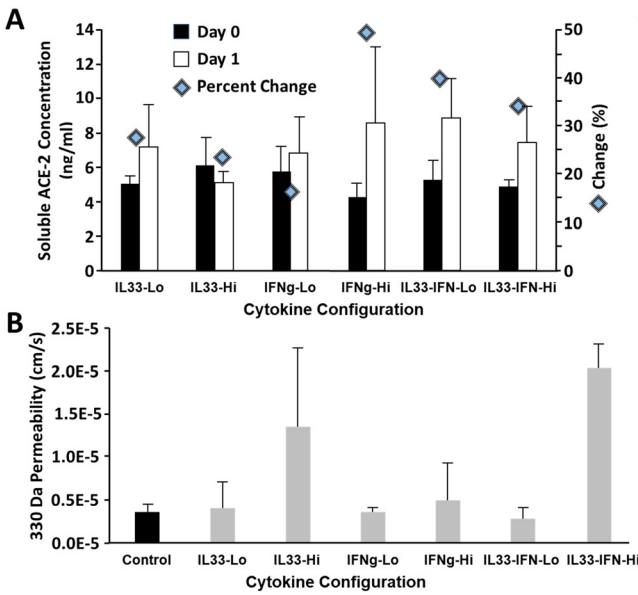

C

	IL-33 (ng/ml)	IFNg (ng/ml)
IL33-Lo	100	
IL33-Hi	1000	
IFNg-Lo		20
IFNg-Hi		100
IL33-IFNg-Lo	100	20
IL33-IFNg-Hi	1000	100

Fig. 6 Effects of Il-33 and IFN-gamma (IFNg) cytokine exposure on the concentration of soluble ACE-2 (sACE-2) in the media withdrawn from a Transwell® (A) and barrier permeability in an airway chip (B). A) The Transwell® concentration of sACE-2 for different concentration combinations of IL-33 and IFNg. The percentage change in concentration was most pronounced for IFNg-Hi, L-33-IFN-Lo, and IL-33-IFN-Hi (N = 4). B) The effects of IL-33 and IFNg on airway chip permeability. The condition that most increased the sACE-2 concentration without loss of barrier function was IL-33-IFNg-Lo (N = 4). C) Table overview of low and high concentrations of cytokines for the six combinations studied.

IL-33, IFN-gamma, or a combination of both (see Fig. 6C) diluted in B-ALI™ Differentiation Media for 24 hours. The commercial ELISA kit that we utilized in our analyses of the media detects the soluble ACE-2 protein (sACE-2) in the media (AbCam Waltham, MA). It is specific to epitopes within the extracellular domain of membrane-bound ACE-2, which during a COVID-19 infection is cleaved from the membrane-bound form and freed from the cells by the disintegrin and metalloprotease 17 (ADAM17) and can serve as a biomarker for COVID-19 infections.[52,53] Fig. 6A shows that the greatest percentage increase in sACE-2 concentration was associated with the IFNg-Hi (100 ng ml^{-1}

IFN-gamma), IL33/IFN-Lo (100 ng ml^{-1} IL-33 + 20 ng ml^{-1} IFN-gamma), and IL33/IFN-Hi (1000 ng ml^{-1} IL-33 + 100 ng ml^{-1} IFN-gamma), resulting in a 49%, 40%, and 34% change in ACE-2 concentration as determined by ELISA. We also assessed the impact of cytokine exposure upon barrier permeability in the airway chip to ensure that treatment did not disrupt cellular functioning. Fig. 6B shows that the IL-33-Hi (1000 ng ml^{-1} IL-33) and IL33/IFN-Hi cohorts were associated with a marked increase in barrier permeability, indicating potential cellular toxicity. The condition that most improved ACE-2 expression without loss of barrier function was low IL-33 + IFN. We could also show that the introduction of activated immune cells could affect airway barrier permeability activation as assessed by cytokine production (Fig. S2).

3.4. Infection with SARS-CoV-2

Having validated the airway model for both physiological relevance for human bronchial airway and suitability for infectious disease testing, we were ready to study infection of the airway model with SARS-CoV-2 in a BSL-3 facility. Chips were allowed to mature for 38 days in BSL-2 before infection in BSL-3. By three days post initial infection, barrier disruption can be seen (N = 3; see Fig. 7A), and plaque assays show successful infection of both the airway and vascular side as early as 24 hours and continuing out to five days (Fig. 7B). Using microscale ELISA from MDS, a panel of 10 cytokines was evaluated over the course of the five-day infection (Table 1), which shows that IL-10 and TNF-α both showed a significance p-value of less than 0.05 on the airway side at the early time points of 24 and 48 hours after infection, but no significant effect was ever observed in the vascular chamber. From these data, three distinct response groups are evident (Fig. 8): one group can be identified by an early response seen only on the airway side, which was the site of infection (Fig. 8A) and is represented by the cytokines TNF-α and interleukin 10. The second response group is one where only the airway side showed strong production (Fig. 8B), represented by interleukin 4, 13, and 12p70. The third is the group of cytokines that showed upregulation for both the airway and the vascular sides, indicating a response to the progression of the infection (Fig. 8C) and represented by interleukin 6, 8, 1β, and INF. Of the 10 cytokines investigated, only interleukin 2 showed relatively no response; however, this cytokine is more strongly associated with T cell activation, and T cells were not included in this model, which may explain the lack of response in interleukin 2. Overall, these proinflammatory cytokines show a pronounced response to SARS-CoV-2 infection, demonstrating that the airway model successfully recapitulates the cytokine storm that has been associated with this infectious disease.

4. Discussion

This paper addresses two issues of current interest: first, we report construction details and operational procedures for a simple gravity-perfused airway chip microphysiological system that is optimized for use under BSL-3 conditions; and second, we demonstrate how this airway chip can be used to quantify the response of a barrier comprised of human bronchial epithelial and human lung microvascular endothelial cells to both SARS-CoV-2 infection and cocktails of inflammatory cytokines. The motivation for this work arose from the rapid emergence of the COVID-19 pandemic and the worldwide spread of SARS-CoV-2 variants that presented a breadth of challenges in diagnosis of the infection, identification of the specific pathogen, characterization of the sequence of events following infection, and determination of the mechanism of action of both the infection and possible therapeutic and prophylactic treatments. While *in vitro* assays for any of these steps that involve active SARS-CoV-2 virus originally had to be performed in a BSL-3 facility, the laboratory biosafety level for SARS-CoV-2 research has now been downgraded to BSL-2. The devices and procedures that we describe are still applicable to the study of other BSL-3 pathogens.

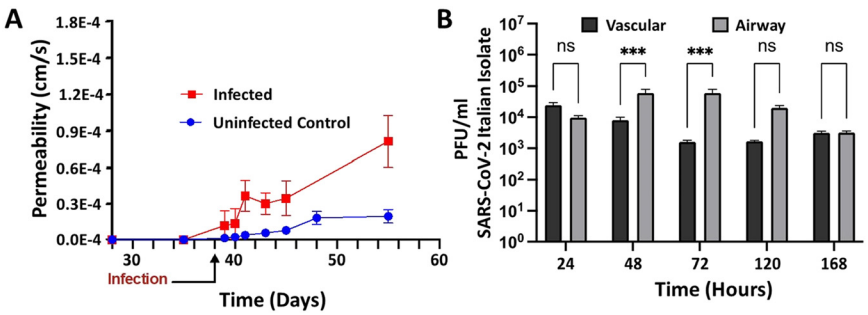

Fig. 7 Airway chip permeability and viral load in the airway and vascular chambers in the context of SARS-CoV-2 infection. A) Permeability of the gravity airway chip was assessed by quantification of FITC-Dextran levels in the airway and vascular chambers. Units were either infected with SARS-CoV-2 Italian isolate or were uninfected controls. Data are obtained as averages from N = 3 each for infected and control sample. B) Longitudinal quantification of viral load in airway and vascular sides of the infected and control units. Data are obtained as averages from N = 3 each for all samples, and infectious titers are represented as PFU ml^{-1}. Statistical analysis was performed using two-way ANOVA with Dunnett's post-test (***$p < 0.001$, ns = not significant).

Table 1 Quantification of proinflammatory cytokine load in the airway and vascular chambers of the airway chips following SARS-CoV-2 Italian isolate infection. The perfused media from the airway and the vascular sides of the units (infected [N = 3], control, [N = 3]) were collected at 24, 48, 72, 120, and 168 hours post-infection. The amounts of 10 proinflammatory cytokines were analyzed in these samples by multiplexed ELISA, of which data for 10 cytokines (IFN-γ, IL-1β, IL-2, IL-4, IL-6, IL-8, IL-10, IL12-p70, IL13, and TNF-α) are included. Each sample was included in the multiplexed ELISA as technical duplicates and the data were averaged for each analyte at each time point. The overall average of the biological replicates was obtained and represented as pg ml^{-1} concentration for each cytokine. Statistical analysis was carried out using t-test *$p < 0.05$, **$p < 0.01$, ***$p < 0.001$, ****$p < 0.0001$

	Vascular					Airway				
Time (HPI)	24	48	72	120	168	24	48	72	120	168
INF-γ	ns	*	*	ns	ns	***	**	**	ns	ns
IL-1β	***	*	*	*	ns	***	***	**	*	*
IL-2	ns	ns	ns	ns	ns	ns	ns	*	ns	ns
IL-4	ns	ns	*	ns	ns	***	***	**	*	**
IL-6	**	**	**	**	*	***	****	****	****	***
IL-8	***	***	***	***	**	****	****	****	****	ns
IL-10	ns	ns	ns	ns	ns	*	*	ns	ns	ns
IL-12p70	ns	ns	ns	ns	ns	***	**	**	*	**
IL-13	ns	ns	*	ns	ns	****	***	***	**	**
TNF-α	ns	ns	ns	ns	ns	*	*	ns	ns	ns

* = $p < 0.05$, ** = $p < 0.01$, *** = $p < 0.001$, **** = $p < 0.0001$.

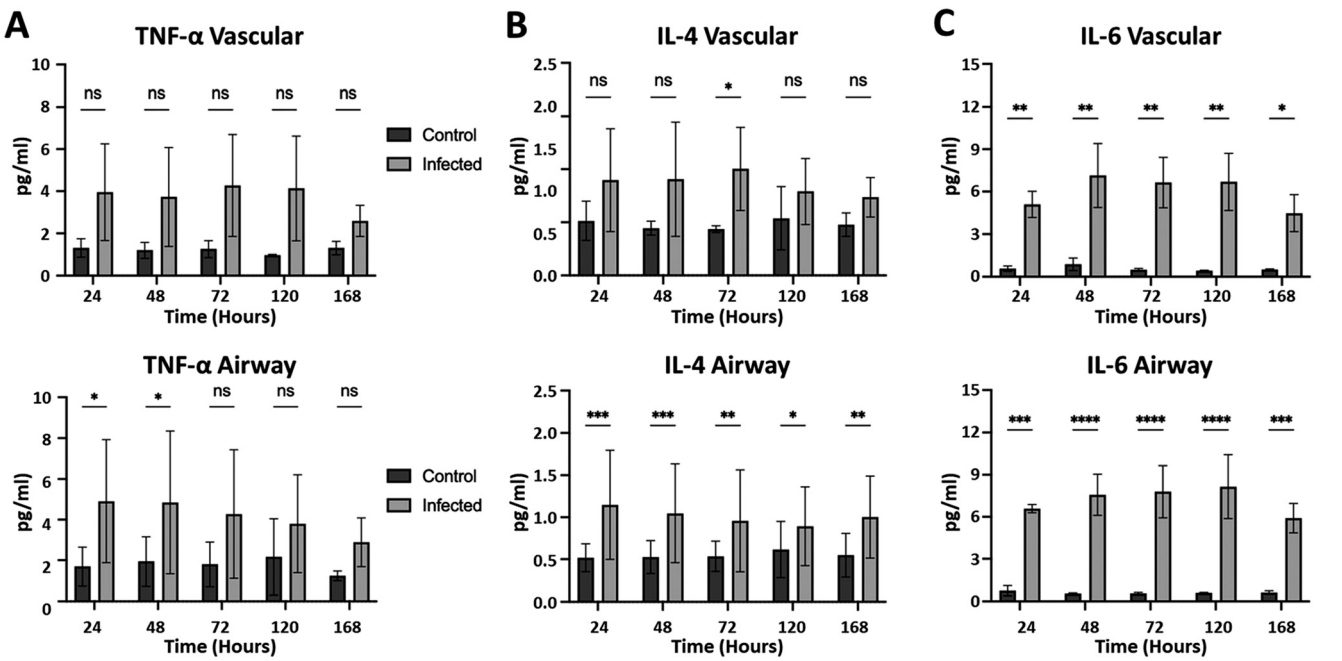

Fig. 8 Representative expression of three different patterns of cytokine response to SARS-CoV-2 infection in airway chips. A) An early response on the airway/infected side that reduces over time. B) Robust cytokine response that is restricted to the airway side alone but maintained throughout the exposure. C) Robust cytokine response on both the airway and the vascular side. Statistical analysis was carried out using t-test *$p < 0.05$, **$p < 0.01$, ***$p < 0.001$, ****$p < 0.0001$.

It is generally recognized that co-culture and barrier MPS models can recapitulate human physiology and pathology more accurately than mono-culture, mono-layer biology on plastic,[7] and we explicitly demonstrated that co-cultures in Transwell® still had significantly reduced barrier function as compared to the MPS chips with the same cells. However, with an increase in the technical demands of the assay there is often a decrease in throughput. The vast majority of MPS studies to date have been conducted in BSL-2 level facilities, which require the assay operator to wear gloves and a lab coat and to open the assay to air only in a HEPA-filtered cell culture biosafety hood, *i.e.*, the same as required for culture of any mammalian cells. The addition of syringe or peristaltic pumps, pressurized reservoirs, or static or dynamic reservoir height differences to drive media flow past cells enclosed in a microfluidic chip is more of an inconvenience than a barrier to the use of MPS chips in standard BSL-2 laboratories, which are essentially designed to protect the cells from the investigator studying them.

One of the generally accepted challenges of using a syringe pump or external pressurized reservoirs to perfuse a microfluidic organ-on-chip, is the need to avoid the introduction of bubbles in the feed lines when connecting a pump or pressurized reservoir to a chip that is already seeded with cells, in that a bubble can effectively scrub cells otherwise adherent to the microfluidic channel. This problem can be addressed in several ways, for example by precise experimental technique, the insertion of microfluidic bubble traps between the pump/reservoir and the chip,[54–56] the use of rocking well plates with open reservoirs,[57] or by the development of well plates with integrated reservoirs and pumps.[32,33,58] In a gravity-perfused organ chip such as ours, the addition of media to a large, open supply reservoir or removal from a collection reservoir can be done without the introduction of bubbles, and without the complexity of tethering an organ chip to an external perfusion system. This problem occurs in conventional BSL-2 laboratories and is aggravated in BSL-3 because of the awkwardness of additional layers of personal protective gear and cramped space.

In contrast to conventional BSL-2 studies of living cells, the study of active microbial and viral agents that can infect humans and for which there are no effective prophylactic or therapeutic treatments, must be conducted in a BSL-3 facility, which protects not only the cells but also the investigators. In addition to the BSL-2 requirements, in BSL-3 investigators must be double-gloved and wear masks and more effective eye protection, and all biowaste and used laboratory supplies must be decontaminated, typically by incineration.[12–16] Equipment maintenance and repair cannot involve simply removing the equipment from the BSL-3 space, repairing it, and later returning it to BSL-3. Equipment that is inoperable, obsolete, or simply no longer needed must be incinerated or otherwise thoroughly decontaminated. These requirements and the typically severe space constraints within a BSL-3 laboratory often discourage the introduction of complex and expensive instruments. Finally, BSL-3 facilities have stringent restrictions on the handling of fluids that could have been exposed to infective agents. For example, a typical cell culture flask must at all times reside within a secondary containment vessel such that spills or splashes cannot contaminate the culture hoods, incubators, bench tops, instruments, floors, or personnel. The BSL-3 requirement for secondary containment of potentially infectious fluids complicates any system where the device under study is physically separated from pumps or pressurized reservoirs and connected by fluid-filled tubing that can be disconnected or damaged. Additional concerns with operating in a BSL-3 or higher cell culture space include getting bulky equipment into and possibly out of the facility, and whether space requirements for secondary confinement for rockers, perfusion systems, or external pumps or pressurized reservoirs might limit the number of studies that can be conducted in parallel.

In designing our organ chip, we sought not only to make something possible, but also practical, robust, and reliable. Our design of a gravity-powered MPS enables both the study of SARS-CoV-2 and Venezuelan equine encephalitis virus (VEEV), and it can be rapidly adapted for new, emerging diseases in the future, thus preventing the time lag that affected research during the recent pandemic. In Fig. 2 and the associated text, we provide a simple yet detailed recipe that should enable other investigators to modify their organ chip devices for prolonged studies in a BSL-3 environment. For our airway chip to contribute something new, it needed to require no scaffolding, no powered rocking machine, and no tubing so that we could maintain a high level of secondary containment and throughput, which are limited by bulkier approaches, and streamline the ease of use so that laboratories that are not experienced with microfluidic systems could benefit from the technology and use their expertise in infectious disease or critical requirements for our chip design. After designing a BSL-3-compatible, gravity-perfused airway chip and completing perfusion testing, our first goal in validation was to demonstrate the ability to culture and generate a fully differentiated, polarized airway epithelial layer. To do so, we utilized multiple cell-surface staining markers as indicators of maturation,[11] including cadherin-26, which has been shown to localize to the airway surface near ciliary membranes and support polarity,[59] and VANGL1, which is strongly associated with a planar-polarized ciliated epithelium.[60,61] The presence of mucin-producing goblet cells was confirmed with mucin 5 AC staining.[62] We were also able to show evidence of possible ciliation.[63] Taken together, these results strongly support the development of mature epithelium within the airway chip.

As we intended these organ chips for use in the fight against COVID-19, we also understood the importance of the expression of ACE-2, which is particularly relevant since it had been shown that although Vero cells not expressing ACE-2 could become infected with SARS-CoV-2, this different mechanism of infection provided poor concurrence with human drug trials.[3] Through both immunohistochemistry and ELISA, we were able to demonstrate increases in the concentration of sACE-2 and to show how modulation of cytokine activity could affect sACE-2 with or without changes to vascular permeability. The final stage of validation showed that we could maintain physiologically relevant permeability[64,65] over at least 30 days in culture.

Having succeeded in validating our novel airway chip, we were ready to test its reliability for modeling infectious disease by infecting it with SARS-CoV-2 in an actual BSL-3 space with live virus. While some groups have conducted studies using pseudoviruses or BSL-2-appropriate coronaviruses,[24,66,67] these options obviously come with limitations with regard to providing direct information on SARS-CoV-2 itself. By utilizing the Italian strain of SARS-CoV-2 and demonstrating the ability to transfer the chips into a BSL-3 space, we were able to establish both infection of the airway epithelium and a transfer of infection to the airway endothelium, resulting in a marked increase in proinflammatory cytokines from both spaces within the airway chip and thus recapitulating key features of COVID-19

in a human cell-based airway chip. Early infection of the airway epithelium was characterized by upregulation of IL-10 and TNF-α. TNF-α has been implicated in assisting viral infection,[68] and IL-10 has been associated with the early phase of COVID-19 infection;[68] thus, the airway chip is accurately mimicking the human response. In the case of the cytokinesis, upregulation was limited to the airway epithelial side. The cytokines IL-4 and 13 have been implicated in lung remodeling in response to COVID-19,[68] as well as in the cytokine storm that includes IL-12p20.[68] Finally, there are four cytokines that show significant upregulation, and both the airway epithelial and the vascular endothelial of the airway chip, and serum concentrations of IL-8, IL-6, and IL-1β have all been shown to have correlations with disease progression or severity, thus indicating their presence in the vascular tissue.[68,69] Given both the spatial and temporal expression of specific cytokine signatures that closely parallel those found in patients suffering from COVID-19 infections, we believe that this platform shows real potential for use not only in better understanding the consequences of SARS-CoV-2 infection, but also as a platform for novel therapeutics for SARS-CoV-2 as well as other viral agents that can enter the body through the airways, including those that have been weaponized for biological warfare, or by other means. This has been partially realized with our success in using this organ chip platform to study VEEV infection.[70]

We recognize that there are numerous ways to address the MPS-in-BSL-3 problem. The greatest limitations of the approach we present are that the flow rates cannot be adjusted without fabricating a chip with different channel dimensions, and the reservoirs need to be serviced every day. We have devised, but not implemented, solutions to these problems.[71]

5. Conclusions

We have demonstrated the ability to produce a microphysiological airway model consisting of a vascular component and a mature epithelial component, with the ability to introduce circulating immune components. We have validated this model's physiological function and its suitability for studies of SARS-CoV-2 infection by demonstrating both the expression of a permeability maturation marker and an increase in sACE-2. We have also shown that this airway model is capable of establishing a SARS-CoV-2 infection that leads to the production of a wave of cytokines reminiscent of the cytokine storm seen in human subjects. Furthermore, we have filled the need for a model system that is compatible with the restrictions placed on a BSL-3 environment, yet can be used easily and interchangeably in any other cell culture environment. By creating a human cell-based airway chip and demonstrating its ability to recapitulate key features of COVID-19 infection, we hope that this will be a useful platform in drug and intervention testing as novel strains of this and other respiratory pathogens continue to challenge vaccines.

Author contributions

Shannon L. Faley: investigation, validation, formal analysis, data curation, writing – original draft, writing – review & editing. Niloufar A. Boghdeh: investigation, validation, formal analysis, data curation, writing – original draft, writing – review & editing. David K. Schaffer: conceptualization, resources, data curation, writing – review & editing. Eric C. Spivey: conceptualization, resources, writing – review & editing. Farhang Alem: conceptualization, methodology, validation, writing – review & editing, supervision. Aarthi Narayanan: conceptualization, methodology, validation, writing – review & editing, supervision, project administration, funding acquisition. John P. Wikswo: conceptualization, methodology, validation, writing – review & editing, supervision, project administration, funding acquisition. Jacquelyn A. Brown: conceptualization, investigation, methodology, validation, formal analysis, data curation, writing – original draft, writing – review & editing, supervision, project administration.

Conflicts of interest

There are no conflicts to declare.

Data availability

Supplementary information (SI): a tabular overview of the antibodies used for immunohistochemistry, a figure showing the layout of the photolithographic mask used to create the microfluidic channels, and a figure that demonstrates the introduction and validation of an immune component to the airway chip. The data supporting this article have been included as part of the article and SI. See DOI: **https://doi.org/10.1039/D5LC00510H**.

Acknowledgements

This work has been supported in part by the Defense Threat Reduction Agency (HDTRA11810040 and HDTRA1-23-1-0003 to AN, and CBMXCEL-XL1-2-001 through a subaward from Los Alamos National Laboratory to JPW), the National Institutes of Health National Center for Advancing Translational Sciences (U01TR002383 to JPW) and the National Center for Advancing Translational Sciences, the National Institute of Neurological Disorders and Stroke, and Eunice Kennedy Shriver National Institute of Child Health and Human Development (UH3TR002097 to JPW). The content is solely the responsibility of the authors and does not necessarily represent the official views of the National Institutes of Health or the Defense Threat Reduction Agency. We are indebted to Monika Judge and Clayton Britt at Vanderbilt for their assistance in the fabrication of the microfluidic, gravity-perfused airway chips, Dr. Shirit Einav of Stanford University for providing the Vero E6-TMPRSS2 cells, and Robin Trundy at Vanderbilt for her clarification of BSL-2 and BSL-3 requirements. We owe a special debt of gratitude to the anonymous reader who identified the errors in the

original paper, and to the editors of *Lab on a Chip*, who recognized that the errors did not affect the conclusions of our study and allowed us to resubmit a corrected paper for review. Last but not least, we appreciate the diligence and comments of the external reviewers.

References

1 M. Xie, X. S. Liu, X. P. Cao, M. Z. Guo and X. C. Li, *Respir. Res.*, 2020, **21**, 49.
2 D. A. Lagowala, S. Kwon, V. K. Sidhaye and D. H. Kim, *Am. J. Physiol.*, 2021, **321**, L1072–L1088.
3 N. S. Ogando, T. J. Dalebout, J. C. Zevenhoven-Dobbe, R. Limpens, Y. van der Meer, L. Caly, J. Druce, J. J. C. de Vries, M. Kikkert, M. Barcena, I. Sidorov and E. J. Snijder, *J. Gen. Virol.*, 2020, **101**, 925–940.
4 B. K. Park, D. Kim, S. Park, S. Maharjan, J. Kim, J. K. Choi, M. Akauliya, Y. Lee and H. J. Kwon, *Biomol. Ther.*, 2021, **29**, 273–281.
5 S. Ramirez, C. Fernandez-Antunez, A. Galli, A. Underwood, L. V. Pham, L. A. Ryberg, S. Feng, M. S. Pedersen, L. S. Mikkelsen, S. Belouzard, J. Dubuisson, C. Solund, N. Weis, J. M. Gottwein, U. Fahnoe and J. Bukh, *Antimicrob. Agents Chemother.*, 2021, **65**, DOI: **10.1128/aac.00097-21**.
6 M. R. Alexander, C. T. Schoeder, J. A. Brown, C. D. Smart, C. Moth, J. P. Wikswo, J. A. Capra, J. Meiler, W. B. Chen and M. S. Madhur, *FASEB J.*, 2020, **34**, 15946–15960.
7 D. E. Watson, R. Hunziker and J. P. Wikswo, *Exp. Biol. Med.*, 2017, **242**, 1559–1572.
8 A. N. Michi and D. Proud, *Am. J. Physiol.*, 2021, **321**, L263–L279.
9 W. Shin, C. D. Hinojosa, D. E. Ingber and H. J. Kim, *iScience*, 2019, **15**, 391–406.
10 T. Pasman, D. Baptista, S. van Riet, R. K. Truckenmuller, P. S. Hiemstra, R. J. Rottier, N. M. Hamelmann, J. M. J. Paulusse, D. Stamatialis and A. A. Poot, *Membranes*, 2021, **11**, 197.
11 E. K. Vladar, J. V. Nayak, C. E. Milla and J. D. Axelrod, *JCI Insight*, 2016, **1**, e88027.
12 *Laboratory biosafety manual*, World Health Organization, 4th edn, 2020, **https://www.who.int/publications/i/item/9789240011311**.
13 *Biosafety in Microbiological and Biomedical Laboratories (BMBL)*, Centers for Disease Control and Prevention, 6th edn, 2020, **https://www.cdc.gov/labs/BMBL.html12**.
14 L. Bane, Inspection Checklist for BSL-3 Laboratories, **https://www.selectagents.gov/compliance/docs/checklists/BSL-3.pdf**, **https://www.selectagents.gov/compliance/preparing.htm**, (accessed 2023-08-11, 2023).
15 NIH Design Requirements, **https://orf.od.nih.gov/TechnicalResources/Documents/DRM/DRMDeskGuide.pdf**, (accessed Aug. 11, 2023).
16 NIH Design Requirements Manual, **https://orf.od.nih.gov/TechnicalResources/Documents/DRM/DRM1.503262020.pdf**, (accessed Aug. 11, 2023).
17 D. Huh, H. Fujioka, Y. C. Tung, N. Futai, R. Paine, J. B. Grotberg and S. Takayama, *Proc. Natl. Acad. Sci. U. S. A.*, 2007, **104**, 18886–18891.
18 D. Huh, B. D. Matthews, A. Mammoto, M. Montoya-Zavala, H. Y. Hsin and D. E. Ingber, *Science*, 2010, **328**, 1662–1668.
19 A. Jain, R. Barrile, A. D. van der Meer, A. Mammoto, T. Mammoto, K. De Ceunynck, O. Aisiku, M. A. Otieno, C. S. Louden, G. A. Hamilton, R. Flaumenhaft and D. Ingber, *Clin. Pharmacol. Ther.*, 2018, **103**, 332–340.
20 K. Schimek, S. Frentzel, K. Luettich, D. Bovard, I. Rütschle, L. Boden, F. Rambo, H. Erfurth, E. M. Dehne, A. Winter, U. Marx and J. Hoeng, *Sci. Rep.*, 2020, **10**, 7865.
21 L. L. Si, H. Q. Bai, M. Rodas, W. J. Cao, C. Y. Oh, A. D. Jiang, R. Moller, D. Hoagland, K. Oishi, S. Horiuchi, S. Uhl, D. Blanco-Melo, R. A. Albrecht, W. C. Liu, T. Jordan, B. E. Nilsson-Payant, I. Golynker, J. Frere, J. Logue, R. Haupt, M. McGrath, S. Weston, T. Zhang, R. Plebani, M. Soong, A. Nurani, S. M. Kim, D. Y. Zhu, K. H. Benam, G. Goyal, S. E. Gilpin, R. Prantil-Baun, S. P. Gygi, R. K. Powers, K. E. Carlson, M. Frieman, B. R. TenOever and D. E. Ingber, *Nat. Biomed. Eng.*, 2021, **5**, 815–829.
22 A. Mori, M. Vermeer, L. J. van den Broek, J. Heijmans, A. Nicolas, J. Bouwhuis, T. Burton, K. Matsumura, K. Ohashi, S. Ito and B. Kramer, *Sci. Rep.*, 2024, **14**, 26248.
23 M. T. Raimondi, F. Donnaloja, B. Barzaghini, A. Bocconi, C. Conci, V. Parodi, E. Jacchetti and S. Carelli, *Theranostics*, 2020, **10**, 7034–7052.
24 J. F. Tan, Q. W. Guo, L. L. Tian, Z. D. Pei, D. F. Li, M. X. Wu, J. H. Zhang and X. H. Gao, *Eur. J. Pharm. Sci.*, 2023, **180**, 106329.
25 M. Zhang, P. Wang, R. H. Luo, Y. Q. Wang, Z. Y. Li, Y. Q. Guo, Y. L. Yao, M. H. Li, T. T. Tao, W. W. Chen, J. B. Han, H. T. Liu, K. L. Cui, X. Zhang, Y. T. Zheng and J. H. Qin, *Adv. Sci.*, 2021, **8**, 2002928.
26 P. Zamprogno, S. Wüthrich, S. Achenbach, G. Thoma, J. D. Stucki, N. Hobi, N. Schneider-Daum, C. M. Lehr, H. Huwer, T. Geiser, R. A. Schmid and O. T. Guenat, *Commun. Biol.*, 2021, **4**, 168.
27 T. Cao, C. M. Shao, X. Y. Yu, R. P. Xie, C. Yang, Y. L. Sun, S. H. Yang, W. J. He, Y. Xu, Q. H. Fan and F. F. Ye, *Research*, 2022, **2022**, 9819154.
28 P. Wang, L. Jin, M. Zhang, Y. S. Wu, Z. L. Duan, Y. Q. Guo, C. M. Wang, Y. Q. Guo, W. W. Chen, Z. Y. Liao, Y. Q. Wang, R. Lai, L. P. Lee and J. H. Qin, *Nat. Biomed. Eng.*, 2023, 1053–1068.
29 T. P. Buzhdygan, B. J. DeOre, A. Baldwin-Leclair, T. A. Bullock, H. M. McGary, J. A. Khan, R. Razmpour, J. F. Hale, P. A. Galie, R. Potula, A. M. Andrews and S. H. Ramirez, *Neurobiol. Dis.*, 2020, **146**, 105131.
30 R. X. Z. Lu, B. F. L. Lai, N. Rafatian, D. Gustafson, S. B. Campbell, A. Banerjee, R. Kozak, K. Mossman, S. Mubareka, K. L. Howe, J. E. Fish and M. Radisic, *Lab Chip*, 2022, **22**, 1171–1186.
31 V. V. Thacker, K. Sharma, N. Dhar, G. F. Mancini, J. Sordet-Dessimoz and J. D. McKinney, *EMBO Rep.*, 2021, **22**, e52744.
32 L. Lopez Quezada, F. Mba Medie, R. J. Luu, R. B. Gaibler, E. P. Gabriel, L. D. Rubio, T. J. Mulhern, E. E. Marr, J. T. Borenstein, C. R. Fisher and A. L. Gard, *Adv. Biol.*, 2024, **8**, 2300511.
33 C. R. Fisher, F. M. Medie, R. J. Luu, R. B. Gaibler, T. J. Mulhern, C. R. Miller, C. J. Zhang, L. D. Rubio, E. E. Marr, V. Vijayakumar, E. P. Gabriel, L. L. Quezada, C. H. Zhang, K. S.

Anderson, W. L. Jorgensen, J. W. Alladina, B. D. Medoff, J. T. Borenstein and A. L. Gard, *Cells*, 2023, **12**, 2639.
34 M. Gerigk, H. Bulstrode, H. H. Shi, F. Tönisen, C. Cerutti, G. Morrison, D. Rowitch and Y. Y. S. Huang, *Lab Chip*, 2021, **21**, 2343–2358.
35 J. A. Brown, V. Pensabene, D. A. Markov, V. Allwardt, M. D. Neely, M. Shi, C. M. Britt, O. S. Hoilett, Q. Yang, B. M. Brewer, P. C. Samson, L. J. M. McCawley, M. James, D. J. Webb, D. Li, A. B. Bowman, R. S. Reiserer and J. P. Wikswo, *Biomicrofluidics*, 2015, **9**, 054124.
36 J. A. Brown, S. G. Codreanu, M. Shi, S. D. Sherrod, D. A. Markov, M. D. Neely, C. M. Britt, O. S. Hoilett, R. S. Reiserer, P. C. Samson, L. J. McCawley, D. J. Webb, A. B. Bowman, J. A. McLean and J. P. Wikswo, *J. Neuroinflammation*, 2016, **13**, 306.
37 J. A. Brown, S. L. Faley, Y. Shi, K. M. Hillgren, G. A. Sawada, T. K. Baker, J. P. Wikswo and E. S. Lippmann, *Fluids Barriers CNS*, 2020, **17**, 38.
38 J. P. Wikswo, F. E. Block III, D. E. Cliffel, C. R. Goodwin, C. C. Marasco, D. A. Markov, D. L. McLean, J. A. McLean, J. R. McKenzie, R. S. Reiserer, P. C. Samson, D. K. Schaffer, K. T. Seale and S. D. Sherrod, *IEEE Trans. Biomed. Eng.*, 2013, **60**, 682–690.
39 J. P. Wikswo, *Exp. Biol. Med.*, 2014, **239**, 1061–1072.
40 C. G. Alver, E. Drabbe, M. Ishahak and A. Agarwal, *Nat. Commun.*, 2024, **15**, 5118.
41 N. A. Boghdeh, K. H. Risner, M. D. Barrera, C. M. Britt, D. K. Schaffer, F. Alem, J. A. Brown, J. P. Wikswo and A. Narayanan, *Viruses*, 2022, **14**, 2799.
42 C. O. Lizama and A. C. Zovein, *Exp. Cell Res.*, 2013, **319**, 1247–1254.
43 T. S. Frost, L. A. Jiang, R. M. Lynch and Y. Zohar, *Micromachines*, 2019, **10**, 533.
44 T. S. Frost, L. A. Jiang and Y. Zohar, *Micromachines*, 2020, **11**, 536.
45 S. Lechuga, A. Marino-Melendez, N. G. Naydenov, A. Zafar, M. B. Braga-Neto and A. I. Ivanov, *Cells*, 2024, **13**, 370.
46 M. Fiorentino, M. M. Levine, M. B. Sztein and A. Fasano, *PLoS One*, 2014, **9**, e85211.
47 H. H. Hsu, J. K. Kracht, L. E. Harder, K. Rudnik, G. Lindner, K. Schimek, U. Marx and R. Pörtner, *J. Visualized Exp.*, 2018, **132**, e56412.
48 S. Lukassen, R. L. Chua, T. Trefzer, N. C. Kahn, M. A. Schneider, T. Muley, H. Winter, M. Meister, C. Veith, A. W. Boots, B. P. Hennig, M. Kreuter, C. Conrad and R. Eils, *EMBO J.*, 2020, **39**, e105114.
49 P. Verdecchia, C. Cavallini, A. Spanevello and F. Angeli, *Eur. J. Intern. Med.*, 2020, **76**, 14–20.
50 E. C. Lin and C. H. Hong, *Biomedicines*, 2022, **10**, 1183.
51 J. Heuberger, J. Trimpert, D. Vladimirova, C. Goosmann, M. Q. Lin, R. Schmuck, H. J. Mollenkopf, V. Brinkmann, F. Tacke, N. Osterrieder and M. Sigal, *EMBO Mol. Med.*, 2021, **13**, e13191.
52 M. Lebedin, C. Ratswohl, A. Garg, M. Schips, C. V. García, L. Spatt, C. Thibeault, B. Obermayer, J. Weiner, III, I. M. Velásquez, C. Gerhard, P. Stubbemann, L. G. Hanitsch, T. Pischon, M. Witzenrath, L. E. Sander, F. Kurth, M. Meyer-Hermann and K. de la Rosa, *iScience*, 2024, **27**, 109330.
53 J. Q. Wang, H. Y. Zhao and Y. Z. An, *Front. Cell. Infect. Microbiol.*, 2022, **11**, 789180.
54 A. M. Skelley and J. Voldman, *Lab Chip*, 2008, **8**, 1733–1737.
55 J. H. Sung and M. L. Shuler, *Biomed. Microdevices*, 2009, **11**, 731–738.
56 C. Lochovsky, S. Yasotharan and A. Gunther, *Lab Chip*, 2012, **12**, 595–601.
57 M. B. Esch, J. M. Prot, Y. I. Wang, P. Miller, J. R. Llamas-Vidales, B. A. Naughton, D. R. Applegate and M. L. Shuler, *Lab Chip*, 2015, **15**, 2269–2277.
58 A. L. Gard, R. J. Luu, R. Maloney, M. H. Cooper, B. P. Cain, H. Azizgolshani, B. C. Isenberg, J. T. Borenstein, J. Ong, J. L. Charest and E. M. Vedula, *Commun. Biol.*, 2023, **6**, 92.
59 M. E. Lachowicz-Scroggins, E. D. Gordon, A. Wesolowska-Andersen, N. D. Jackson, H. J. MacLeod, L. Z. Sharp, M. Sun, M. A. Seibold and J. V. Fahy, *Cell Discovery*, 2018, **4**, 7.
60 M. T. Butler and J. B. Wallingford, *Development*, 2015, **142**, 3429–3439.
61 D. Devenport, *J. Cell Biol.*, 2014, **207**, 171–179.
62 K. A. Knoop and R. D. Newberry, *Mucosal Immunol.*, 2018, **11**, 1551–1557.
63 P. Ziegler, Y. R. Tian, Y. L. Bai, S. Abrahamsson, A. Backerholm, A. S. Reznik, A. Green, J. A. Moore, S. E. Lee, M. M. Myerburg, H. J. Park, K. W. Tang and K. H. Y. Shair, *PLoS Pathog.*, 2021, **17**, e1009041.
64 H. X. Lin, H. Li, H. J. Cho, S. Bian, H. J. Roh, M. K. Lee, J. S. Kim, S. J. Chung, C. K. Shim and D. D. Kim, *J. Pharm. Sci.*, 2007, **96**, 341–350.
65 N. R. Mathias, J. Timoszyk, P. I. Stetsko, J. R. Megill, R. L. Smith and D. A. Wall, *J. Drug Targeting*, 2002, **10**, 31–40.
66 A. J. McAuley, P. J. van Vuren, M. U. R. Mohammed, Faheem, S. Goldie, S. Riddell, N. J. Godde, I. K. Styles, M. P. Bruce, S. Chahal, S. Keating, K. R. Blasdell, M. Tachedjian, C. M. O'Brien, N. B. Singanallur, J. N. Viana, A. V. Vashi, C. M. Kirkpatrick, C. A. MacRaild, R. M. Shah, E. Vincan, E. Athan, D. J. Creek, N. L. Trevaskis, S. Murugesan, A. Kumar and S. S. Vasan, *Viruses*, 2022, **14**, 2417.
67 J. W. Yang, Y. R. Lin, Y. L. Chu, J. H. Y. Chung, H. E. Lu and G. Y. Chen, *Commun. Biol.*, 2022, **5**, 70.
68 S. Haga, N. Yamamoto, C. Nakai-Murakami, Y. Osawa, K. Tokunaga, T. Sata, N. Yamamoto, T. Sasazuki and Y. Ishizaka, *Proc. Natl. Acad. Sci. U. S. A.*, 2008, **105**, 7809–7814.
69 Y. M. Chang, M. R. Bai and Q. H. You, *BioMed Res. Int.*, 2022, **2022**, 2755246.
70 S. Saul, K. E. Huie, C. Tindle, M. Sibai, C. J. Ye, A. M. Khalil, K. Chiem, L. Martinez-Sobrido, J. M. Dye, B. A. Pinsky, P. Ghosh, S. Das, D. E. Solow-Cordero, J. Jin, J. P. Wikswo, D. Jochmans, J. Neyts, S. De Jonghe, A. Narayanan, S. Einav, M. Karim, L. Ghita, P. T. Huang, W. Chiu, V. Duran, C. W. Lo, S. Kumar, N. Bhalla, P. Leyssen, F. Alem, N. A. Boghdeh, D. Tran, C. A. Cohen and J. A. Brown, *J. Clin. Invest.*, 2023, **133**, e169510.

71 D. K. Schaffer, J. P. Wikswo, R. S. Reiserer, M. D. Geuy, E. C. Spivey, C. M. Britt, J. A. Brown, D. A. Markov, S. Faley, L. J. McCawley and P. C. Samson, WIPO Patent Application, WO2021/222778A1, 2021.